Journal of Power Sources 195 (2010) 5637–5644

Contents lists available at ScienceDirect

Journal of Power Sources

journal homepage: www.elsevier.com/locate/jpowsour

Operation of solid oxide fuel cells on glycerol fuel: A thermodynamic analysis using the Gibbs free energy minimization approach

Aline Lima da Silva*, Iduvirges Lourdes Müller

Program of Postgraduate Studies in Mining, Metals and Materials Engineering (PPGEM), Federal University of Rio Grande do Sul, UFRGS, Campus do Vale, Setor 4, Prédio 75, Sala 226, Av. Bento Gonçalves 9500, CEP 91501-970, Porto Alegre, RS, Brazil

ARTICLE INFO

Article history:
Received 3 March 2010
Received in revised form 23 March 2010
Accepted 23 March 2010
Available online 30 March 2010

Keywords:
Solid oxide fuel cells
Direct utilization
Glycerol
Electrochemical thermodynamics
Carbon deposition
Gibbs energy minimization method

ABSTRACT

Solid oxide fuel cells (SOFCs) are very flexible, unlike other fuel cells. In principle, SOFCs can operate on almost any fuel. Currently much effort is invested in the development of SOFCs for portable applications operating directly on liquid fuels such as methanol and ethanol rather than hydrogen. However, there are very few publications dealing with the direct use of glycerol in SOFCs for portable systems. A recently published study shows that the performance achieved for an SOFC fueled by pure glycerol is quite interesting even when there is a thick electrolyte membrane, indicating that glycerol is a promising fuel for portable applications. For this reason a thermodynamic analysis for SOFCs operating directly on glycerol fuel is performed in the present study. The Gibbs energy minimization method computes the equilibrium compositions of the anode gas mixture, carbon deposition boundaries and electromotive forces (EMFs) as a function of fuel utilization and temperature. Moreover, the minimum amounts of H_2O, CO_2 (direct internal reforming case) and air (partial oxidation case) to be added to glycerol in the feedstock to avoid carbon deposition at the open circuit voltage (OCV) are calculated. Finally, a thermodynamic analysis is performed, taking into account the experimental conditions employed in a previous study. Experimental observations concerning carbon deposition in an SOFC operating on glycerol can be explained by the theoretical analysis developed in the present study. Additionally, the effect of mixed electronic–ionic conduction of the electrolyte on carbon deposition at the anode is discussed based on the thermodynamic analysis of the C–O system.

1. Introduction

Solid oxide fuel cells (SOFCs) are regarded as a promising source of clean and efficient electricity generation [1]. A major advantage of SOFCs is that they potentially have great fuel flexibility, which in principle may allow operation on any combustible fuel [2]. Moreover, SOFCs have a great potential as portable electric generators and as energy sources for transportation. The simplicity afforded by not having to reform the hydrocarbon fuels is a significant advantage of these cells [3]. In fact, the portable applications of SOFCs have been recently extended [4–7]. For these applications, selecting a proper fuel is a crucial step for its commercialization. Such a fuel should be cheap, safe and easy to store and transport [5]. In this context, methanol and ethanol have been considered promising candidate fuels for portable SOFC applications, since both have a very low impurity content and are oxygenated, which reduces the risks of poisoning and may reduce carbon deposition if used in SOFCs [6–8].

However, there are very few reports about SOFCs operating directly on glycerol. In a recent work, Lo Faro et al. [9] experimentally investigated the electrochemical oxidation of glycerol ($C_3H_8O_3$) as an alternative to hydrogen and methane at an intermediate temperature SOFC (IT-SOFC) by using a noble metal-free anode catalyst. It was found that the SOFC cell showed suitable power density especially under anhydrous conditions (327 mW cm^{-2}, at 1073 K). The performance achieved for pure glycerol was quite interesting even in the presence of a thick electrolyte membrane (250 μm). Hence, glycerol could also be a promising candidate for portable SOFC applications.

It could also be mentioned that only a small amount of glycerol from the biodiesel production is purified for use in the food, pharmaceutical, tobacco and cosmetic industries, so the majority is simply wasted. Consequently, with increased production of biodiesel, a glut of glycerol is expected on the world market [10]. Therefore it is important to find efficient and effective uses for glycerol.

Glycerol is a green chemical (non-toxic, non-volatile and non-flammable) which makes it ideal for a wide variety of power uses. It has also high energy density (6.260 kWh L^{-1} for the pure liquid) making it a very attractive fuel for energy purposes [11]. Besides,

* Corresponding author. Tel.: +55 51 3308 9404.
E-mail address: adasilva26@gmail.com (A. Lima da Silva).

0378-7753/$ – see front matter © 2010 Elsevier B.V. All rights reserved.
doi:10.1016/j.jpowsour.2010.03.066

Nomenclature

G	total Gibbs energy of the system
G_i^0	Gibbs energy of species i in its standard state
n_i	number of moles of species i
n_i^0	initial number of moles of species i
n_i'	decision variable during the optimization process, after the change of variables
$\exp(n_i')$	number of moles of species i, after the change of variables
y_i	mole fraction of species i
R	gas constant
T	temperature of the system
P	total pressure of the system
a_i	activity of species i
M, N	total number of components and species, respectively
p_i	partial pressure of species i
μ_i	chemical potential of species i
λ_C	Lagrange's multiplier related to the elemental mass balance of carbon
CDB	carbon deposition boundary
CGO	gadolinia-doped ceria electrolyte
OCV	open circuit voltage
α_{ik}	number of atoms of kth element present in each molecule of species i
b_k	total number of atomic masses of kth element in the system
b_O^{echem}	additional number of moles of oxygen (O) in the system, due to the electrochemical reaction
D_{gra}	chemical driving force for nucleation of graphite phase
U_f	operating fuel utilization (%)
F	Faraday constant (96,485.34 C mol^{-1})
E	electromotive force of cell (V) for reversible conditions
K_{H_2O}	equilibrium constant of hydrogen oxidation
j	current density
t_{ion}	transference number of oxygen ions
z	number of electrons produced per glycerol molecule

Superscripts

an.	anode
cat.	cathode

glycerol is oxygenated, like methanol and ethanol. Hence, the direct oxidation of glycerol in SOFCs to produce electricity is of interest, due to its wide availability and to its renewable character.

To the best of our knowledge, there is no thermodynamic study on the direct utilization of glycerol in SOFCs. Thus, the purpose of the study reported here is to obtain the equilibrium compositions of the anode gas mixture, carbon deposition boundaries and electromotive forces (EMFs) as a function of fuel utilization and temperature. Moreover, the minimum amounts of H_2O, CO_2 (direct internal reforming case) and air (partial oxidation case) to be added to glycerol in the feedstock to avoid carbon deposition at the open circuit voltage (OCV) are calculated. It is relevant to establish ranges of operating conditions at which carbon formation is thermodynamically unfavorable, because it is known that deposited carbon covers the active anode sites, resulting in rapid, irreversible cell deactivation [12].

There are few theoretical studies dealing with the influence of the degree of oxidation of a fuel on the equilibrium composition of the anode gas mixture. Cimenti and Hill [8] performed a thermodynamic analysis for direct utilization of alcohol fuels (methanol and ethanol) in SOFCs. Since their theoretical analysis provides a general treatment of the equilibrium for SOFCs fueled by oxygenated hydrocarbons, the work of these authors was used as a guide for the present study.

Furthermore, thermodynamic analysis is conducted taking into account the same conditions employed by Lo Faro et al. [9]. In this way, experimental observations reported by these authors, regarding carbon deposition during the operation of an SOFC on glycerol fuel, are explained by the thermodynamic approach developed in the present work.

2. Methodology

2.1. Theoretical background

For a system in which many simultaneous reactions take place, equilibrium calculations are performed through the Gibbs energy minimization method. The total free energy of the system, composed of an ideal gas phase and pure condensed phases, may be expressed as

$$\frac{G}{RT} = \left(\sum_{i=1}^{N} n_i \left[\frac{G_i^0}{RT} + \ln(y_i P) \right] \right)_{gas} + \frac{1}{RT} \left(\sum_{i=1}^{N} n_i G_i^0 \right)_{condensed} \quad (1)$$

The problem consists in finding the different values of n_i which minimize the objective function given by Eq. (1), subject to the constraints of elemental mass balance:

$$\sum_{i=1}^{N} n_i \alpha_{ik} = b_k \quad k = 1 \ldots M \quad (2)$$

Based on previous experimental work [13–15], the following species were considered in the simulations: glycerol, acetaldehyde, ethylene, ethanol, methanol, ethane, propylene, acetone, acrolein formaldehyde, allyl alcohol, propionaldehyde, acetic acid (the ideal gas phase), and C (graphite), as a pure condensed phase. Thus, $M = 3$ (C, H and O). The thermodynamic data necessary for describing the Gibbs energy of the species were obtained from Refs. [16–19]. Besides, $P = 1$ atm throughout this work.

The non-linear programming model comprising the objective function to be minimized and constraints is solved by the Solver function contained in the Microsoft Excel spreadsheet package. A thermodynamic analysis for ethanol steam reforming in a reformer using the Solver tool was done in a previous study [20], and the results obtained were satisfactory. Nevertheless, one should take into account the fact that when the Solver applies the Generalized Reduced Gradient (GRG) algorithm, it seems to violate the non-negativity constraints. In order to overcome this drawback, a change of variables was proposed ($n_i = \exp(n_i')$). Thus, no difficulty is caused by the involvement of logarithmic functions of the objective function and there is no need to add non-negativity constraints. The value of 1×10^{-10} was chosen as a criterion of precision and convergence in the Solver Options dialog box during the optimization process.

When an SOFC is producing a current, there is a net input of oxygen ions (O^{2-}) to the anodic compartment that changes the equilibrium conditions of the system. Thus, moles of oxygen must be added to the elemental mass balance of oxygen (O), as shown in Eq. (3). While b_O corresponds to the moles of oxygen in the system, obtained from the inlet feed mixture at the anode, b_O^{echem} is the extra number of moles of oxygen due to the electrochemical reaction:

$$\sum_{i=1}^{N} n_i \alpha_{iO} = b_O + b_O^{echem} \quad (3)$$

Fuel utilization (U_f) is related to b_O^{echem} as follows:

$$b_O^{echem} = 0.5 z U_f n^0_{glycerol} \quad (4)$$

where z is the number of electrons produced by the oxidation of 1 glycerol molecule (14 electrons).

The number of moles of oxygen available at the anode, for complete diffusion of the oxygen ions from the cathode to the anode, through the dense electrolyte, can be calculated using Faraday's Law:

$$b_O^{echem}\ (\text{mol cm}^{-2}\,\text{s}^{-1}) = \frac{j}{2F} \quad (5)$$

where j is the current density in A cm^{-2} and F is Faraday's constant. Combining Eqs. (4) and (5), current density can be related to fuel utilization:

$$j = zFU_f n^0_{glycerol} \quad (6)$$

The reversible electrical potential difference across the electrolyte of an SOFC can be calculated as follows [21]:

$$E = \frac{RT}{2F} \ln \frac{p^{an.}_{H_2} \cdot K_{H_2O} \cdot (p^{cat.}_{O_2})^{0.5}}{p^{an.}_{H_2O}} \quad (7)$$

The value of $p^{cat.}_{O_2}$ is 0.206 atm. K_{H_2O} is the equilibrium constant of the reaction of hydrogen oxidation. It is necessary to stress that Eq. (7) is true in the ideal case of a pure ionic electrolyte, where $t_{ion} = 1$. t_{ion} is the transference number of oxygen ions which is defined as the ratio of ionic conductivity to total conductivity. If the electrolyte shows non-negligible electronic conduction, it is preferable to use the Wagner Equation [22]:

$$E = \frac{RT}{4F} \int_{p^{cat.}_{O_2}}^{p^{an.}_{O_2}} t_{ion} d\ \ln p_{O_2} \quad (8)$$

2.2. Carbon deposition conditions

Carbon activity in the equilibrium system (a_C) can be readily computed, with no need to consider any chemical reaction regarding carbon formation, simply by using the following mathematical relationship [20]:

$$\ln a_C = \left(\frac{-G^0_C}{RT}\right) + \frac{\lambda_C}{RT} \quad (9)$$

After the optimization process is completed, the Lagrange's multiplier related to the elemental mass balance of the element C (λ_C) can be obtained from the sensitivity reports created by the Solver tool. If carbon activity (with reference to the graphite phase) is smaller than unity, carbon formation is thermodynamically impossible. On the other hand, if $a_C = 1$, the system is in a state of equilibrium, and carbon is present along with the gas phase. Finally, when $a_C > 1$, the system is a metastable gas phase and carbon deposition should occur.

As carbon deposition is undesirable, conditions under which carbon starts to disappear are established. At fixed temperature, a given parameter (e.g. fuel utilization, amount of H_2O, CO_2 or air) is varied, and the carbon activity is monitored. The carbon deposition boundary (CDB) is defined as the value of the parameter whose corresponding a_C is approaching the unity. If the value of the operational parameter is greater than that indicated at the CDB, carbon formation in the equilibrium mixture is thermodynamically impossible, because, under these conditions, $a_C < 1$.

The tendency for carbon deposition can also be evaluated through the chemical driving force. At a given temperature, the driving force for carbon deposition with reference to the graphite phase, D_{gra}, can be calculated as follows:

$$D_{gra} = RT \ln a_C \quad (10)$$

Carbon activity values greater than unity can be computed if the graphite phase is excluded both from the total Gibbs free energy of the system and from the constraints of the elemental mass balance of carbon. Therefore, the positive driving force for the nucleation of the graphite phase may be determined.

3. Results and discussion

3.1. Glycerol pyrolysis

Fig. 1(a) and (b) shows the equilibrium composition as a function of temperature for glycerol pyrolysis. As can be seen, the main species present at equilibrium are H_2, CO, CO_2, CH_4, H_2O and C (graphite). Glycerol is completely decomposed over the whole temperature range. Table 1 shows that other species do not exist in the equilibrium mixture from a practical viewpoint. As shown in Fig. 1(a), carbon deposition is predicted over the entire temperature range. Under the operational conditions of IT-SOFCs, i.e. 773–1073 K, the concentration of carbon decreases from 26.3 to 3.34 mol%. Fig. 1(b) shows that the production of H_2 and CO is favored by a temperature increase whereas the concentration of CH_4 and H_2O decreases as temperature increases. This behavior may be attributed to the endothermic steam reforming of methane ($CH_4 + H_2O = CO + 3H_2$). At 1073 K, the anode gas phase is composed of ~55 vol.% of H_2 and ~39 vol.% of CO. Besides, the concentration of CO_2 in the anode gas phase decreases as temperature increases. Such a trend may be explained by the endothermic dry reforming of CH_4 ($CH_4 + CO_2 = 2CO + 2H_2$) [23]. With increase in temperature, the H_2 to CO (H_2/CO) ratio approaches 1.3 (1.333 ...). At 1223 K, the H_2/CO ratio is ~1.332, $n_{CO} = 2.932$ and $n_{H_2} = 3.907$. This indicates that the direct decomposition of glycerol to H_2 and CO ($C_3H_8O_3 = 3CO + 4H_2$) is the predominant reaction at high temperatures. At elevated temperatures, methanol was also found to decompose mainly into H_2 and CO ($CH_3OH = CO + 2H_2$) [8]. Such a similarity may be ascribed to the fact that both fuels are oxygenated hydrocarbons having a C:O ratio equal to 1:1 [24].

As seen in Fig. 1(a), the amount of carbon decreases as temperature increases. This is in accordance with the temperature dependence of the driving force for the nucleation of graphite (Fig. 2). $D_{gra} > 0$ and $a_C > 1$ over the entire temperature range, indicating the thermodynamic feasibility of carbon formation.

Table 1
Gas-phase concentrations (vol.%) at 773, 923 and 1073 K, computed for glycerol pyrolysis.

	Temperature (K)		
	773	923	1073
Glycerol	1.5×10^{-27}	5.5×10^{-27}	5.2×10^{-28}
Acetaldehyde	2.1×10^{-9}	8.2×10^{-9}	5.9×10^{-9}
Ethylene	1.2×10^{-6}	1.1×10^{-5}	2.7×10^{-5}
Ethanol	1.4×10^{-10}	1.7×10^{-10}	3.8×10^{-11}
Methanol	2.4×10^{-7}	3.9×10^{-7}	1.5×10^{-7}
Ethane	1.7×10^{-4}	6.9×10^{-5}	1.4×10^{-5}
Propylene	8.6×10^{-10}	5.3×10^{-9}	7.8×10^{-9}
Acetone	1.6×10^{-11}	2.6×10^{-11}	7.4×10^{-12}
Acrolein	2.7×10^{-10}	1.2×10^{-8}	5.1×10^{-8}
Formaldehyde	1.6×10^{-6}	1.4×10^{-5}	2.5×10^{-5}
Allyl alcohol	1.4×10^{-16}	2.1×10^{-15}	2.8×10^{-15}
Propionaldehyde	1.2×10^{-12}	3.8×10^{-12}	1.8×10^{-12}
Acetic acid	1.2×10^{-8}	6.3×10^{-9}	5.5×10^{-10}

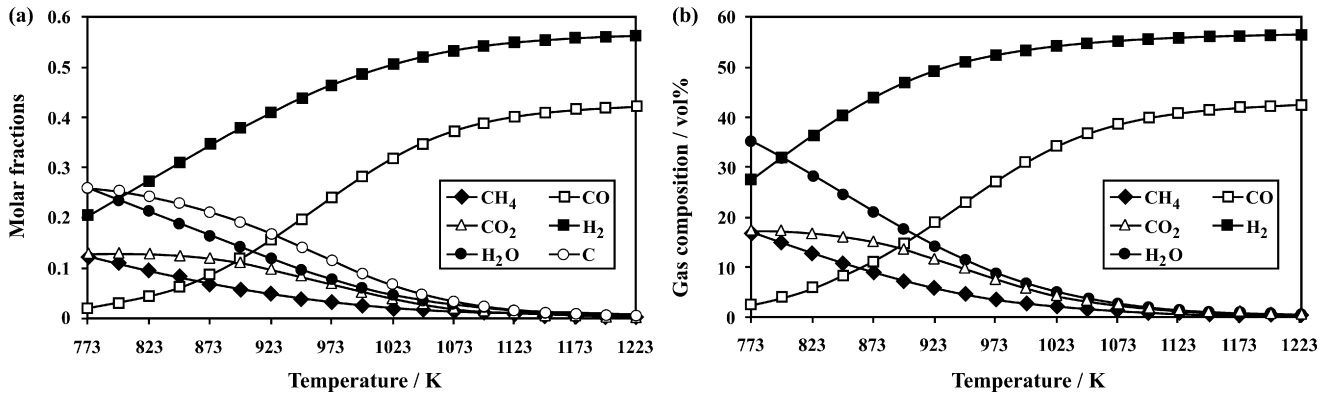

Fig. 1. (a) Molar fractions of the species at the anode as a function of temperature and (b) gas-phase concentrations as a function of temperature.

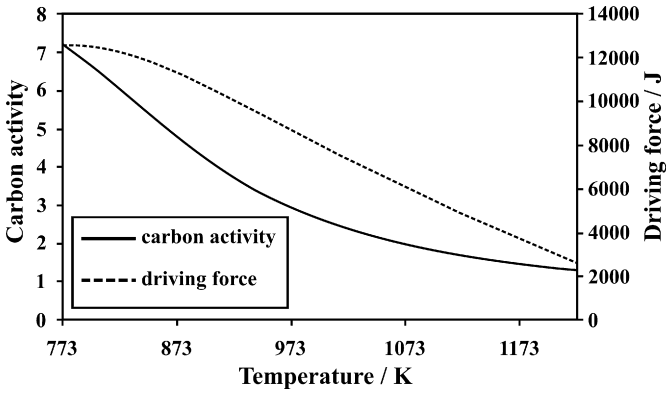

Fig. 2. Carbon activity and driving force for the nucleation of the graphite phase as a function of temperature.

3.2. Effect of fuel utilization and current density on carbon deposition

Fig. 3(a)–(d) shows the equilibrium composition of the main species (H_2, CO, CO_2, H_2O, CH_4 and C (graphite)) and EMFs as a function of fuel utilization, at 773, 873, 973 and 1073 K, respectively, for an SOFC operating on pure glycerol. For instance, the equilibrium compositions and EMFs are also shown as a function of current density, assuming that the anode is fueled with a practical flow rate corresponding to the fuel stoichiometry required by the Faradaic process when the SOFC operates at 1 A cm^{-2} (thus, 7.4×10^{-7} mol s^{-1} of pure glycerol). The amount of carbon is maximal at the OCV. Carbon concentration decreases with increased load up to a fuel utilization beyond which carbon deposition is no longer thermodynamically favored (CDB). Up to the CDB, carbon activity is equal to unity. After the CDB, the driving force for carbon deposition becomes increasingly negative. It may be observed that the minimum fuel utilization in an SOFC fed on pure glycerol to operate in the carbon free region decreases as temperature increases. At high temperatures, the values computed for fuel utilization at the CDB are close to those reported for SOFCs operating on pure methanol [8]. For instance, at 1073 K, the U_f values at the CDB are 3.6 and 2.1% for glycerol and methanol, respectively. The current density at which carbon is reduced to zero (CDB) is known as threshold current density [25,26]. For the conditions examined here, the threshold current densities are 564, 392, 159 and 36 mA cm^{-2}, at 773, 873, 973 and 1073 K, respectively. The molar fraction of CO increases within the carbon deposition region, while it decreases after the threshold current density. Up to the CDB, H_2 exists at a constant concentration and there is little increase in H_2O. After the CDB, H_2 decreases, and the concentration of H_2O increases significantly. Carbon dioxide concentration increases with fuel utilization. At higher temperatures, however, its production increases abruptly after the threshold current density (Fig. 3(c)–(d)). The amount of methane is almost zero for the entire fuel utilization range at 1073 K. At lower temperatures, methane concentration is constant up to the CDB. After the CDB, its concentration decreases rapidly as U_f increases. The OCVs are 1.029, 1.032, 1.048 and 1.080 V at 773, 873, 973 and 1073 K, respectively. Besides, EMFs decrease with fuel utilization. Fuel components might be, in principle, fully utilized in an SOFC. However, the maximum value of U_f examined here is 80% to obtain a reasonable value of EMF, e.g., 0.88 V at 1073 K. Besides, in practice, the acceptable level of partial pressure of residual hydrogen is around 0.1 atm (~80%U_f) [27]. Lower values may result in high concentration overpotentials. The trends seen in Fig. 3(a)–(d), for the species and EMFs, are very similar to those observed in previous work [8,25,26].

It is worthwhile pointing out that all these predictions depend on favorable kinetics, since carbon is not easily removed once formed [28]. Moreover, the carbon deposition boundary is determined assuming that the stable configuration of the system may be reached, with no kinetic impediments. Nevertheless, the equilibrium situation may not always occur. One deviation from equilibrium, for instance, concerns the incomplete conversion of glycerol and the formation of intermediate species. Therefore, there may be more carbon than predicted.

3.3. Direct internal reforming and partial oxidation of glycerol

As shown in Fig. 1(a), at the OCV (U_f = 0%), carbon deposition is predicted over the entire temperature range. Steam, CO_2 or air can be added to glycerol in the feedstock to avoid carbon deposition at the OCV. Fig. 4(a)–(c) shows the minimum amounts of H_2O, CO_2 (direct internal reforming case) and air (partial oxidation case), respectively, needed to prevent carbon deposition as a function of temperature.

The CDB shifts towards lower H_2O/glycerol ratio as temperature increases, in accordance with the results previously shown for glycerol pyrolysis (Fig. 1(a) and 2). Wang et al. [29] computed the CDB for glycerol steam reforming, in the temperature range 550–1000 K. The CDB in Fig. 4(a) shows a satisfactory agreement with the results reported by these authors.

As shown in Fig. 4(b), for temperatures lower than 973 K, high inlet CO_2/glycerol ratios are required to suppress carbon formation. Accordingly, Cimenti and Hill [8] found that large amounts of CO_2 should be added to ethanol or methanol to prevent carbon deposition at lower temperatures. Besides, as in the case of methanol, the CO_2/glycerol ratio approaches zero as temperature increases. By comparing Fig. 4(a) and (b), one can verify that steam is a more effective choice than CO_2 in preventing carbon deposition at low

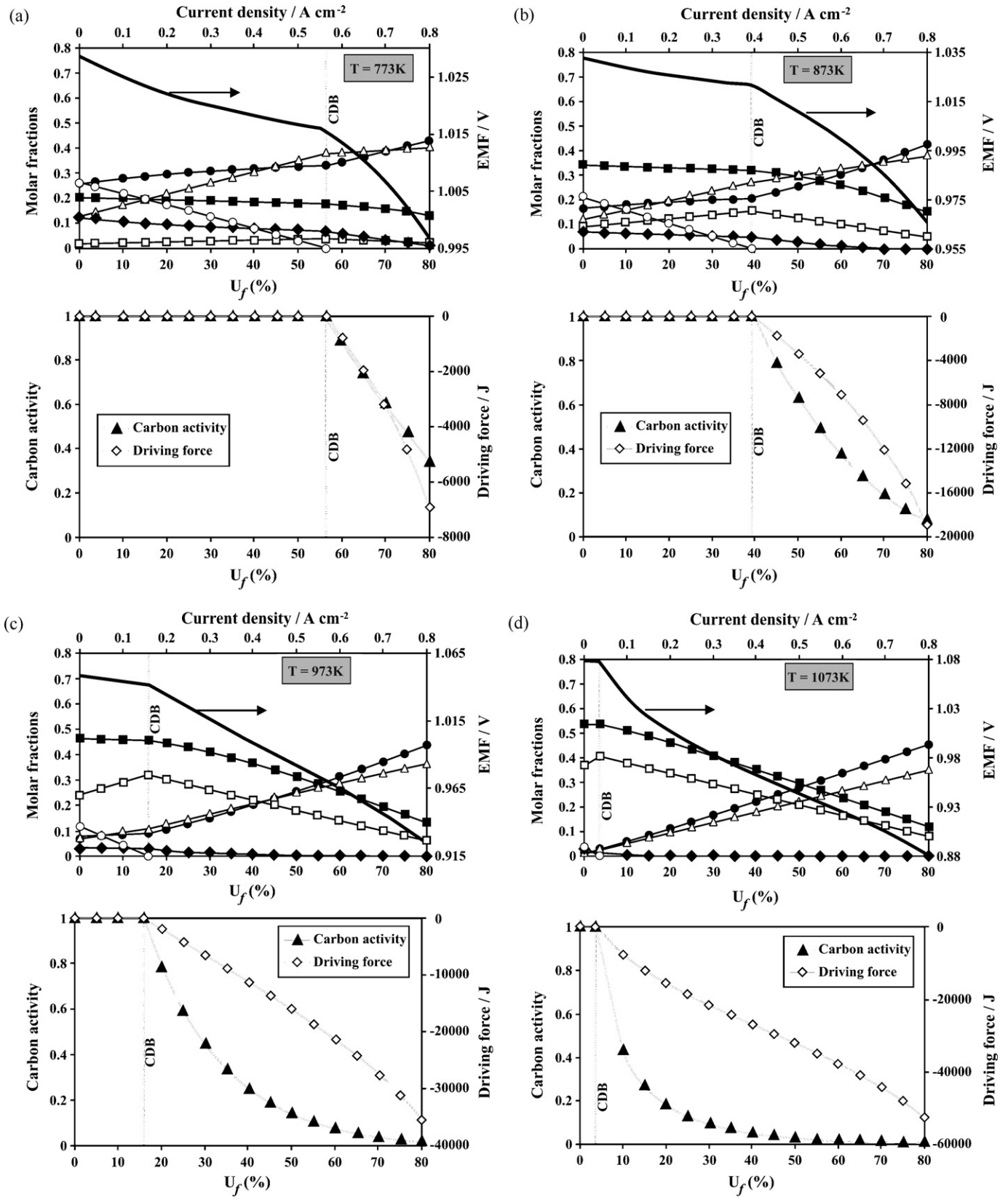

Fig. 3. Calculated equilibrium diagram of carbon (graphite) and the main species in the gas phase and electromotive force as a function of fuel utilization and current density for SOFC anode operating on pure glycerol at 7.4×10^{-7} mol s^{-1}. Carbon activity and driving force as a function of fuel utilization: (a) 773 K, (b) 873 K, (c) 973 K, and (d) 1073 K. The species at equilibrium are: (♦) CH_4, (△) CO_2, (□) CO, (●) H_2O, (○) C (graphite), and (■) H_2.

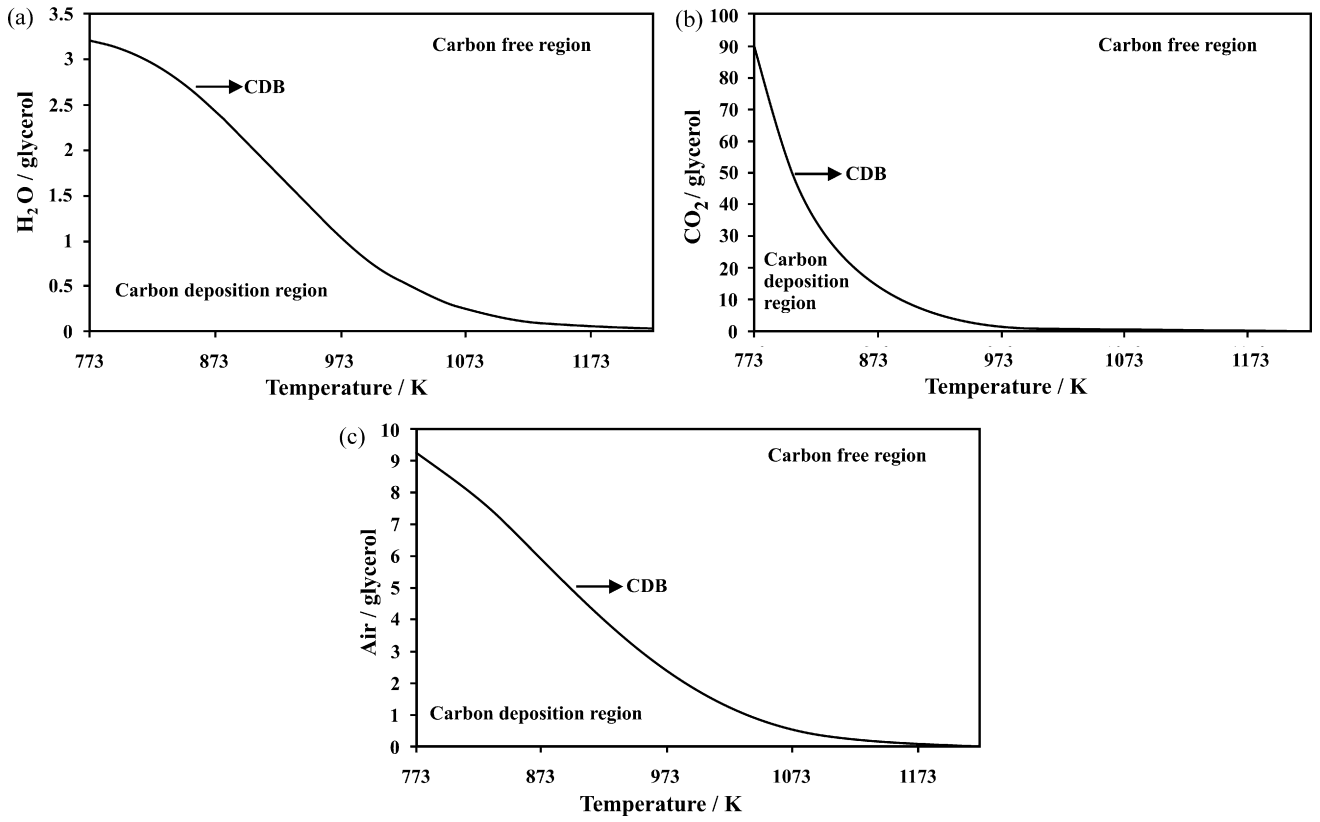

Fig. 4. Carbon deposition boundary (CDB) as a function of temperature for glycerol (a) steam reforming, (b) dry reforming and (c) partial oxidation with air.

temperatures. At higher temperatures, however, CO_2 and steam have a comparable effect.

When air is added (Fig. 4(c)), a similar trend is seen to that of the addition of steam. Steam is a more effective choice, particularly at lower temperatures, due to the higher air/glycerol ratio required compared with the H_2O/glycerol ratio. This is in perfect agreement with the findings of Assabumrungrat et al. [30].

By analyzing the equilibrium compositions calculated at the CDB for direct internal reforming (steam and dry reforming) and partial oxidation with air, it is seen that, in all cases, the H_2/CO ratio approaches 1.3 as temperature increases, indicating that glycerol forms almost exclusively H_2 and CO. Consistently, the number of moles of H_2 approaches 4 and the moles of methane tend to zero.

In practical operation, CO_2 is unlikely to be added to the system for suppressing carbon deposition. Steam and air are more practical additive choices. In principle, the integration of the exothermic heat from partial oxidation with air and the endothermic reforming reactions might make the use of air attractive [30]. Nevertheless, an operating SOFC is strongly exothermic, and the heat released in a fuel cell can provide the heat for internal steam reforming which, under typical operational conditions, is about half the total heat produced [31]. Partial oxidation with air to prevent carbon deposition represents a waste of fuel and an overall inefficient process, because part of the fuel energy is lost due to the exothermic character of this reaction, which lowers the efficiency of the system. However, partial oxidation might be suitable for small-scale portable applications where system simplicity and rapid start-up rather than system efficiency are crucial factors [7]. Although the direct internal reforming approach is an efficient process, simplifying the overall system design, one should take into account the fact that the endothermic reforming reaction on the Ni cermet anode catalyst is so rapid that it causes a strong cooling effect at the fuel entry, leading to inefficient electrochemical kinetics. In this way, partial external steam reforming is the preferred mode of operation, in which waste heat obtained by combusting the anode exit stream in an SOFC operating at ~80% fuel utilization is used.

3.3.1. *Effect of steam content*

Fig. 5 shows the equilibrium diagram with the main species, at 973 K, for the molar flow rate of pure glycerol equal to 7.4×10^{-7} mol s^{-1} and the inlet H_2O/glycerol ratio equal to 2. There is no carbon deposition. This was expected, because this ratio is higher than that indicated at the CDB in Fig. 4(a). The molar fractions of H_2 and CO decrease throughout the range of fuel utilization (or current density) due to possible oxidation to water and carbon dioxide, respectively, which increase continuously as fuel utiliza-

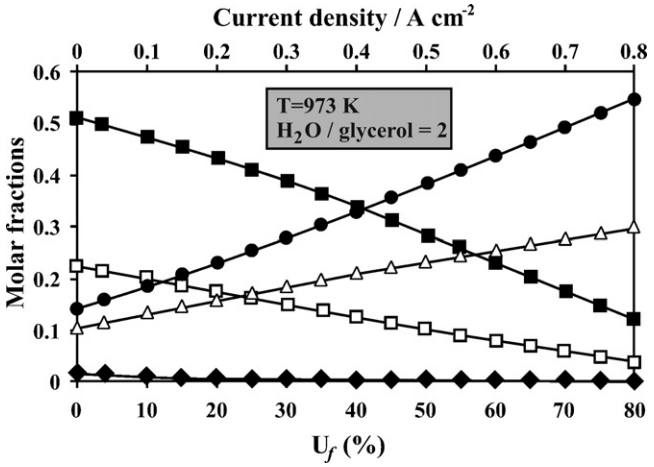

Fig. 5. Equilibrium diagram of the main species as a function of fuel utilization and current density for H_2O/glycerol = 2, at T = 973 K. The species at equilibrium are: (♦) CH_4, (△) CO_2, (□) CO, (●) H_2O and (■) H_2.

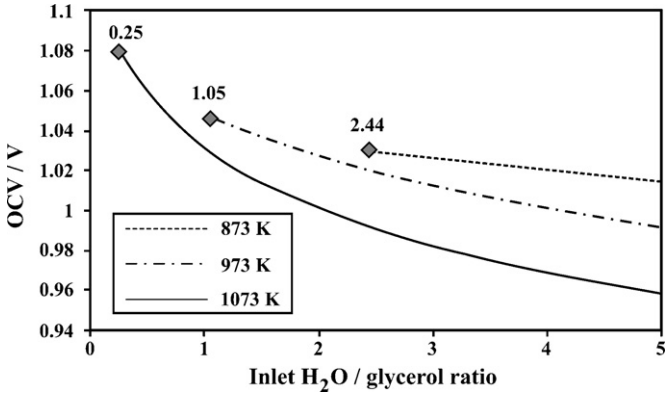

Fig. 6. Open circuit voltage (OCV) as a function of the inlet H_2O/glycerol ratio, at T = 873, 973 and 1073 K. The markers indicate the inlet H_2O/glycerol ratio at the CDB computed for glycerol steam reforming.

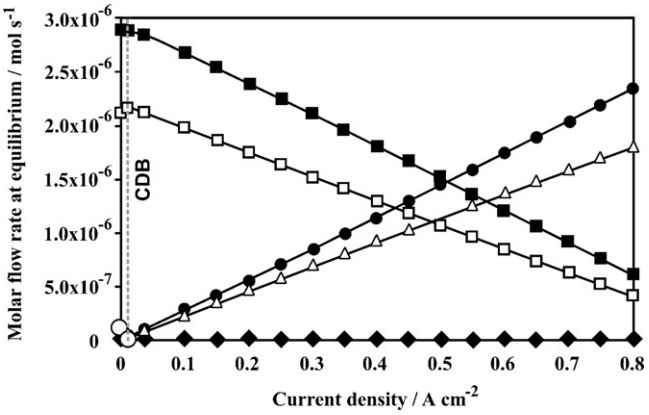

Fig. 7. Equilibrium diagram of carbon (graphite) and the main species in the gas phase as a function of current density for SOFC anode operating on an inlet stream of 7.4×10^{-7} mol s^{-1} of pure glycerol in 20 cm^3 min^{-1} N_2 (carrier gas), at 800 °C. The species at equilibrium are: (♦) CH_4, (△) CO_2, (□) CO, (●) H_2O, (■) H_2 and (○) C (graphite).

tion increases. At 973 K, the molar fraction of methane is almost zero. Note that the trends are similar to those seen in Fig. 3(c) after the threshold current density.

The effect of steam content on the OCV is shown in Fig. 6. The OCV decreases with the inlet H_2O/glycerol ratio. Therefore, if steam is added to the feed stream, the maximum OCV is reached at the carbon deposition boundary.

3.4. Theoretical determination of carbon deposition conditions and comparison with experimental reports

Lo Faro et al. [9] experimentally investigated the electrochemical oxidation of glycerol at 800 °C. The anode was fed on glycerol with a flow rate as close as possible to the fuel stoichiometry required by the Faradaic process when the SOFC operates at 1 A cm^{-2} (7.4×10^{-7} mol s^{-1} of pure glycerol). N_2 carrier gas (20 cm^3 min^{-1}) was used in the glycerol fuel stream. The anode electrocatalyst was based on a Ni-modified $La_{0.6}Sr_{0.4}Fe_{0.8}Co_{0.2}O_3$ (LSFCO) perovskite and gadolinia-doped ceria electrolyte (CGO). The maximum current density is ~0.8 A cm^{-2} based on their polarization curves. These authors stated that no carbon deposits were observed for anodes which had operated in both direct oxidation and internal reforming modes. However, deposited carbon was observed in the alumina tube at the inlet of the stream. Their experimental observations regarding carbon deposition may be explained by thermodynamic analysis. For this purpose, calculations were conducted reflecting the experimental operating conditions adopted by these authors. In this way, two different approaches are considered.

3.4.1. Equilibrium diagram of main species as a function of current density

The molar flow rate of species as a function of current density is shown in Fig. 7. At the OCV (j = 0 A cm^{-2}), carbon deposition is thermodynamically predicted, which is consistent with the observation of the deposited carbon in the alumina tube at the inlet of the stream. As can be seen from this diagram, a very low threshold current density (10.5 mA cm^{-2}) is required to suppress carbon formation under dry conditions, at 800 °C. It may be assumed that the carbon initially formed at the OCV was easily removed, since the threshold current density is much lower than the maximum current density. Thus, even when no steam is added to the feed stream, carbon formation is not possible from a thermodynamic viewpoint under the conditions examined. Indeed, very low values of threshold current density are computed for glycerol, especially at high temperatures. This may be ascribed to its oxygenated character. It is worthwhile pointing out that if methane, for example, were employed under the same conditions, the threshold current density would be much greater (253 mA cm^{-2}). Besides, the addition of the inert gas shifted the threshold current density from 36 to 10.5 mA cm^{-2}. The effect of an inert carrier gas is similar to that obtained with a decrease in total pressure of the system [32]. Thus, if carbon deposition occurs by means of the Boudouard reaction ($C + CO_2 = 2CO$), it is expected that N_2 carrier gas shifts this reaction towards CO, preventing carbon formation, which results in a lower threshold current density.

Lo Faro et al. [9] did not characterize their electrochemical system by impedance spectroscopy technique. Our validation is based on their polarization curve and reports from optical microscopy and CHNS-O analyses. Further experimental work would be very helpful to understand the electrochemical reactions involved in the glycerol oxidation in SOFCs as well as the conditions of carbon deposition.

3.4.2. The effect of mixed electronic–ionic conduction of the electrolyte

The OCV calculated using Eq. (7), considering the equilibrium composition shown in the diagram of Fig. 7 for j = 0 A cm^{-2}, is 1.14 V. Nevertheless, under dry conditions, the experimental value of the OCV is ~0.78 V. This low value can be ascribed to mixed electronic–ionic conduction of the CGO electrolyte, which does not allow the cell to reach high OCVs associated with a very low oxygen partial pressure at the anode [33]. Some mixed conducted electrolytes such as doped CeO_2 are less stable under reduced anodic atmosphere [22]. In fact, the partial pressure of oxygen computed at the OCV was 7.81×10^{-23} atm, corresponding to a strongly reducing atmosphere. Therefore, electronic conduction is expected to appear due to electrons generated by the reduction reactions ($O_O^x = (1/2)O_2 + V_O^{\bullet\bullet} + 2e'$). The electronic defect (e') is due to the Ce reduction ($Ce^{4+} \rightarrow Ce^{3+}$) [33]. For mixed conducted electrolytes, Zha et al. [22] show that the EMF (E) can be calculated as follows:

$$E = \frac{RT}{F} \ln \frac{\left(p^*_{O_2}\right)^{1/4} + \left(p^{cat.}_{O_2}\right)^{1/4}}{\left(p^*_{O_2}\right)^{1/4} + \left(p^{an.}_{O_2}\right)^{1/4}} \quad (11)$$

$p^*_{O_2}$ is an intrinsic property of the electrolyte. The temperature dependence of $p^*_{O_2}$ for the CGO electrolyte was obtained from Kudo and Obayashi [34]. At 1073 K, $p^*_{O_2} = 9.08 \times 10^{-17}$ atm. Thus, the OCV computed by Eq. (11) is 0.81 V, which is close to the experimental value. As a consequence, the thermodynamic possibility of carbon deposition in an atmosphere in which $p_{O_2} = p^*_{O_2}$ should

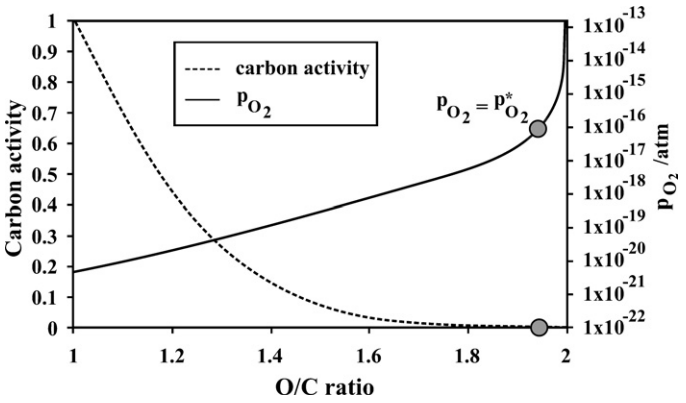

Fig. 8. Carbon activity and partial pressure of O_2 as a function of the O/C ratio, computed for the C–O system at 1073 K.

be analyzed. In this way, the C–O system was studied, and the following species were considered in the Gibbs energy minimization procedure: CO, CO_2, O_2 and C (graphite). Fig. 8 shows that carbon activity decreases as p_{O_2} increases. When p_{O_2} is increased towards $p^*_{O_2}$, carbon activity is only 5×10^{-4}, meaning that carbon deposition is greatly inhibited from a thermodynamic viewpoint. At $p^*_{O_2}$ graphite is oxidized mainly to CO_2. In this way, it can be seen that, at high temperatures, the large availability of oxygen at the anode/electrolyte interface, due to mixed electronic–ionic conduction of the CGO electrolyte, is able to completely oxidize the deposited carbon even at the OCV from a thermodynamic viewpoint.

4. Conclusions

A thermodynamic analysis was performed for the direct utilization of glycerol in SOFCs. The following conclusions can be drawn from the results of the present study:

- H_2 and CO are the main products of glycerol pyrolysis. At high temperatures, the reaction $C_3H_8O_3 = 3CO + 4H_2$ dominates the decomposition equilibrium. Carbon deposition is predicted in the temperature range 773–1223 K. Under the operational conditions of IT-SOFCs (773–1073 K), the concentration of carbon decreases from 26.3 to 3.34 mol%.
- When an SOFC is producing current, carbon deposition becomes thermodynamically less favorable. If the SOFC operates on pure glycerol, at a practical flow rate corresponding to the fuel stoichiometry required by the Faradaic process when the SOFC operates at 1 A cm^{-2}, the threshold current densities are 564, 392, 159 and 36 mA cm^{-2}, at 773, 873, 973 and 1073 K, respectively. At 1073 K, the addition of inert carrier gas to the anode feed stream shifts the threshold current density towards a lower value, preventing carbon formation.
- The minimum amounts of steam, CO_2 and air to be added to glycerol in the feedstock to avoid carbon at the OCV were determined. Steam is a more effective choice than CO_2 mainly at lower temperatures, since very high inlet CO_2/glycerol ratios are required at $T < 973$ K. Air was also found to be less attractive than steam, due to the higher air/glycerol ratio required compared with the H_2O/glycerol ratio. The effect of steam, CO_2 and air on carbon suppression was comparable at high temperatures.
- With respect to the pyrolysis and the direct utilization in SOFCs, glycerol behaves similarly to methanol at high temperatures, which can be ascribed to the fact that both fuels have a C:O ratio equal to 1:1.
- Regarding carbon deposition in an SOFC operating on glycerol, experimental observations may be explained by the theoretical analysis developed in this paper. The combined effect of the oxygenated character of glycerol, which results in very low values of threshold current density at higher temperatures, and the large availability of oxygen at the anode/electrolyte interface, promoted both by the electrochemical reaction during the operation of the SOFC and mixed electronic–ionic conduction of the CGO electrolyte, would seem to prevent irreversible carbon deposition at the anode.
- Although SOFC may not operate at equilibrium, thermodynamic analysis of the decomposition gas compositions and carbon deposition provides a useful guideline for further experimental research. Nevertheless, electrochemical models that consider all overpotentials involved in SOFC operation must be developed. Besides, energy analyses must be performed in order to quantify the optimal operating parameters.

Acknowledgments

The authors thank CNPq and CAPES for financial support.

References

[1] Z. Shao, S.M. Haile, J. Ahn, P.D. Ronney, Z. Zhan, S.A. Barnett, Nature 435 (2005) 795–798.
[2] S. McIntosh, R.J. Gorte, Chem. Rev. 104 (2004) 4845–4866.
[3] S. Park, J.M. Vohs, R.J. Gorte, Nature 404 (2000) 265–267.
[4] P.K. Cheekatamarla, C.M. Finnerty, C.R. Robinson, S.M. Andrews, J.A. Brodie, Y. Lu, P.G. DeWald, J. Power Sources 193 (2009) 797–803.
[5] S. Farhad, F. Hamdullahpur, J. Power Sources 195 (2010) 3084–3090.
[6] M. Cimenti, J.M. Hill, J. Power Sources 195 (2010) 54–61.
[7] M. Cimenti, J.M. Hill, Energies 2 (2009) 377–410.
[8] M. Cimenti, J.M. Hill, J. Power Sources 186 (2009) 377–384.
[9] M. Lo Faro, D. La Rosa, M. Minutoli, G. Monforte, V. Antonucci, A.S. Aricò, ECS Trans. 25 (2) (2009) 2241–2248.
[10] S. Adhikari, S. Fernando, S.R. Gwaltney, S.D. Filip To, R. Mark Bricka, P.H. Steele, A. Haryanto, Int. J. Hydrogen Energy 32 (2007) 2875–2880.
[11] R.L. Arechederra, B.L. Treu, S.D. Minteer, J. Power Sources 173 (2007) 156–161.
[12] B. Huang, X.F. Ye, S.R. Wang, H.W. Nie, J. Shi, Q. Hu, J.Q. Qian, X.F. Sun, T.L. Wen, J. Power Sources 162 (2006) 1172–1181.
[13] T. Valliyappan, N.N. Bakhshi, A.K. Dalai, Bioresour. Technol. 99 (2008) 4476–4483.
[14] W. Buhler, E. Dinjus, H.J. Ederer, A. Kruse, C. Mas, J. Supercrit. Fluids 22 (2002) 37–53.
[15] X. Xu, Y. Matsumura, J. Stenberg, M.J. Antal Jr., Ind. Eng. Chem. Res. 35 (1996) 2522–2530.
[16] C.L. Yaws, Chemical Properties Handbook, McGraw-Hill, New York, 1999.
[17] O. Knacke, O. Kubaschewski, K. Hesselmann, Thermochemical Properties of Inorganic Substances, second ed., Springer-Verlag, Berlin, 1991.
[18] S.I. Sandler, Chemical and Engineering Thermodynamics, third ed., Wiley, New York, 1999.
[19] R.C. Reid, J.M. Prausnitz, B.E. Poling, The Properties of Gases and Liquids, fourth ed., MCGraw-Hill, New York, 1987.
[20] A. Lima da Silva, C.F. Malfatti, I.L. Müller, Int. J. Hydrogen Energy 34 (2009) 4321–4330.
[21] A. Demin, P. Tsiakaras, Int. J. Hydrogen Energy 26 (2001) 1103–1108.
[22] S.W. Zha, C.R. Xia, G.Y. Meng, J. Appl. Electrochem. 31 (2001) 93–98.
[23] A.N. Fatsikostas, D.I. Kondarides, X.E. Verykios, Catal. Today 75 (2002) 145–155.
[24] R.R. Davda, J.W. Shabaker, G.W. Huber, R.D. Cortright, J.A. Dumesic, Appl. Catal. B 56 (2005) 171–186.
[25] J. Mermelstein, M. Millan, N. Brandon, J. Power Sources 195 (2010) 1657–1666.
[26] D. Singh, E. Hernández-Pacheco, P.N. Hutton, N. Patel, M.D. Mann, J. Power Sources 142 (2005) 194–199.
[27] A.K. Demin, P.E. Tsiakaras, V.A. Sobyanin, S.Y. Hramova, Solid State Ionics 152–153 (2002) 555–560.
[28] J.-H. Koh, Y.-S. Yoo, J.-W. Park, H.C. Lim, Solid State Ionics 149 (2002) 157–166.
[29] X. Wang, S. Li, H. Wang, B. Liu, X. Ma, Energy Fuels 22 (2008) 4285–4291.
[30] S. Assabumrungrat, N. Laosiripojana, P. Piroonlerkgul, J. Power Sources 159 (2006) 1274–1282.
[31] P. Aguiar, D. Chadwick, L. Kershenbaum, Chem. Eng. Sci. 57 (2002) 1665–1677.
[32] L. Hernández, V. Kafarov, J. Power Sources 192 (2009) 195–199.
[33] J.H. Joo, G.M. Choi, Solid State Ionics 178 (2007) 1602–1607.
[34] T. Kudo, H. Obayashi, J. Electrochem. Soc. 123 (1976) 415–419.